Model and learning-based computational 3D phase microscopy with intensity diffraction tomography

1st Alex Matlock
Electrical And Computer Engineering
Boston University
Boston, MA, USA
amatlock@bu.edu

2nd Yujia Xue
Electrical And Computer Engineering
Boston University
Boston, MA, USA
yujiaxue@bu.edu

3rd Yunzhe Li
Electrical And Computer Engineering
Boston University
Boston, MA, USA
Emmal@bu.edu

4th Shiyi Cheng
Electrical And Computer Engineering
Boston University
Boston, MA, USA
csy11@bu.edu

5th Waleed Tahir
Electrical And Computer Engineering
Boston University
Boston, MA, USA
waleedt@bu.edu

6th Lei Tian
Electrical And Computer Engineering
Boston University
Boston, MA, USA
leitian@bu.edu

***Abstract*—Intensity Diffraction Tomography (IDT) is a new computational microscopy technique providing quantitative, volumetric, large field-of-view (FOV) phase imaging of biological samples. This approach uses computationally efficient inverse scattering models to recover 3D phase volumes of weakly scattering objects from intensity measurements taken under diverse illumination at a single focal plane. IDT is easily implemented in a standard microscope equipped with an LED array source and requires no exogenous contrast agents, making the technology widely accessible for biological research.**

Here, we discuss model and learning-based approaches for complex 3D object recovery with IDT. We present two model-based computational illumination strategies, multiplexed IDT (mIDT) [1] and annular IDT (aIDT) [2], that achieve high-throughput quantitative 3D object phase recovery at hardware-limited 4Hz and 10Hz volume rates, respectively. We illustrate these techniques on living epithelial buccal cells and *Caenorhabditis elegans* worms. For strong scattering object recovery with IDT, we present an uncertainty quantification framework for assessing the reliability of deep learning-based phase recovery methods [3]. This framework provides per-pixel evaluation of a neural network predictions confidence level, allowing for efficient and reliable complex object recovery. This uncertainty learning framework is widely applicable for reliable deep learning-based biomedical imaging techniques and shows significant potential for IDT.

***Index Terms*—Tomography, High Volume-Rate Imaging, Physics-Based Learning, Uncertainty Learning, Computational Imaging**

I. Introduction

Three-dimensional (3D) quantitative phase imaging (QPI) modalities have gained significant interest in biology for recovering volumetric morphological information of unlabeled samples [4]–[10]. These methods invert the scattered field measured from an illuminated sample for 3D recovery [4] and have shown utility in numerous fields including immuno-oncology [11] and cytopathology [12]. Existing 3D QPI modalities are often interferometric [6], [13], [14] requiring specialized optical setups that can limit their widespread adoption for biological research applications. Recently, intensity-based QPI methods have gained momentum from using simple optical setups [7], [8], [15] with various phase encoding strategies [7], [8], [15]–[20] for object phase recovery. In particular, intensity diffraction tomography (IDT) [8] provides volumetric object recovery using intensity-only measurements and can be implemented in a standard optical microscope equipped with an LED array. The original IDT implementation acquires hundreds of illumination patterns from a rectangular LED array and uses computationally efficient, linear inverse scattering models for recovering high-quality volumetric phase information [8]. Unfortunately, this initial IDT approach suffers from long acquisition time and weakly scattering object limitations that prevent the evaluation of living complex biological specimens. Here, we provide model-based computational illumination strategies for high volume-rate IDT and discuss learning-based methods for reliably and efficiently recovering quantitative volumetric information of complex, multiply-scattered objects.

IDT, like Differential Phase Contrast (DPC) and Fourier Ptychography (FP) [21]–[26], encodes the object's phase into intensity using oblique illumination [7], [8], [18], [22]. These diverse illumination methods provide synthetic aperture-based resolution enhancement [8], [21], [22] and have shown successful high-speed phase recovery using sparse [21], [27] and multiplexed illumination [23], [24], [27]. 3D object recovery with these existing techniques is also possible with sample scanning [15] and more complex models and reconstruction algorithms [7], [10], [28]–[30]. Providing high-speed volumetric recovery of complex, multiple-scattering objects is still a significant challenge for such diverse illumination strategies, however, due to the large datasets and increased computa-

This work was partially supported by National Science Foundation (NSF) (1813848, 1846784) and National Institutes of Health (NIH) (R21GM128020). Alex Matlock acknowledges the National Science Foundation Graduate Research Fellowship (DGE-1840990).

tional complexity required of these approaches. Alternatively, IDT provides an easily implementable 3D recovery approach with model-based computational illumination strategies that enhance the modality's throughput without increased complexity or loss in quality. With the use of learning-based phase recovery, IDT shows significant promise for providing efficient, reliable evaluation of complex 3D objects.

Deep learning (DL) has rapidly expanded as a computationally efficient tool for phase recovery [31]. DL utilizes end-to-end neural network architectures to learn the inverse scattering model or incorporate physics-based approximants or constraints to improve the network's predictions [31]–[35]. While these methods are computationally efficient once trained, the "black box" nature of DL reduces the reliability of these predictions for biological research. Here, we discuss an uncertainty learning framework, applied to the FP modality [3], that quantifies a neural network's per-pixel uncertainty regarding its output phase prediction. This framework is generalizable to different network architectures and shows significant promise for providing reliable 3D object recovery with IDT.

This work discusses model and learning-based techniques enhancing IDT's complex object recovery. We present two computational illumination strategies, multiplexed IDT (mIDT) and annular IDT (aIDT), that use software-only and hardware-only illumination modifications to provide high-quality volumetric reconstructions of dynamic biological samples at hardware-limited 4Hz and 10Hz rates, respectively. We briefly describe these approaches and show their utility on live epithelial buccal cells and *C. elegans* worms. Furthermore, we discuss an uncertainty learning framework providing reliability assessments of neural network-based phase recovery. We show these approaches can enhance the capabilities of the IDT technique and expand the technology to evaluating thick, multiply-scattering dynamic biological samples.

II. Technique Overview

We provide a brief IDT model overview highlighting its key parameters for the model-based illumination techniques in Section III. The full model is discussed elsewhere [8].

The IDT physical model assumes the object of interest, defined by a scattering potential $O(\boldsymbol{r}) = \frac{k_0^2}{4\pi}\Delta\epsilon(\boldsymbol{r})$ with wavenumber k_0, permittivity contrast $\Delta\epsilon(\boldsymbol{r}) = \epsilon_{obj}(\boldsymbol{r}) - \epsilon_0$ with the surrounding homogeneous imaging medium ϵ_0, and spatial position $\boldsymbol{r}$, generates weak scattering from an incident field following the first Born approximation [36]. The total field $u_{tot}(\boldsymbol{r})$ from an incident plane wave $u_i(\boldsymbol{r}|\boldsymbol{\nu_i})$ with lateral spatial frequency $\boldsymbol{\nu}_i$ interacting with such an object has the form

$$u_{tot}(\boldsymbol{r}|\boldsymbol{\nu}_i) = u_0(\boldsymbol{r}|\boldsymbol{\nu}_i) + \int_V u_0(\boldsymbol{r'})O(\boldsymbol{r'})G(\boldsymbol{r}-\boldsymbol{r'})d\boldsymbol{r'} \quad (1)$$

where $G(\boldsymbol{r})$ is the free-space Green's function and V is the object volume. This approximation assumes the scattered fields generated throughout the object's volume are mutually *independent* and *linearly* related to the object's features. Under these assumptions, the object can be discretized into axial slices (Fig. 1(a)) each providing unique phase information at the image plane. Given the proper model, these object slices can be recovered from diverse illumination measurements at a single focal plane.

IDT provides a linear physical forward model relating the measured intensity spectra to the underlying object. This spectra contains four terms (Fig. 1(a)): 1) The self-interfered incident field background signal $\hat{I}_1$, 2) the incident and scattered field cross-interference with its complex conjugate ($\hat{I}_2$, $\hat{I}_3$), and 3) the self-interfered scattered field ($\hat{I}_4$). $\hat{I}_2$ and $\hat{I}_3$ preserve the linearity between the measured intensity and the object's permittivity contrast and are used for IDT's linear model. Assuming $\hat{I}_1$ can be removed computationally through a background subtraction and $\hat{I}_4$ is negligible under weakly scattering conditions, the IDT model becomes $\hat{I}(\boldsymbol{\nu}|\boldsymbol{\nu}_i) \approx H_{\mathrm{re}}\Delta\epsilon_{\mathrm{re}} + H_{\mathrm{im}}\Delta\epsilon_{\mathrm{im}}$ for an object with complex permittivity contrast $\Delta\epsilon(\boldsymbol{r}) = \Delta\epsilon_{re}(\boldsymbol{r}) + j\Delta\epsilon_{im}(\boldsymbol{r})$. The model's transfer functions (TFs), simplified from [8], have the form

$$H_{\mathrm{re}}(\boldsymbol{\nu}, q|\boldsymbol{\nu}_i) \propto j\Big\{P(\boldsymbol{\nu}^-)\frac{e^{-j\Phi(\boldsymbol{\nu}^-,\boldsymbol{\nu}_i)q\Delta z}}{\eta(\boldsymbol{\nu}^-)} - P(\boldsymbol{\nu}^+)\frac{e^{j\Phi(\boldsymbol{\nu}^+,\boldsymbol{\nu}_i)q\Delta z}}{\eta(\boldsymbol{\nu}^+)}\Big\}, \quad (2a)$$

$$H_{\mathrm{im}}(\boldsymbol{\nu}, q|\boldsymbol{\nu}_i) \propto \Big\{P(\boldsymbol{\nu}^-)\frac{e^{-j\Phi(\boldsymbol{\nu}^-,\boldsymbol{\nu}_i)q\Delta z}}{\eta(\boldsymbol{\nu}^-)} + P(\boldsymbol{\nu}^+)\frac{e^{j\Phi(\boldsymbol{\nu}^+,\boldsymbol{\nu}_i)q\Delta z}}{\eta(\boldsymbol{\nu}^+)}\Big\}, \quad (2b)$$

where $P(\boldsymbol{\nu})$ is the system's pupil function, $\boldsymbol{\nu}^{\pm} = \boldsymbol{\nu} \pm \boldsymbol{\nu}_i$ is the lateral spatial frequency shifted by the illumination angle, $\eta(\boldsymbol{\nu}) = \sqrt{(1/\lambda)^2 - |\boldsymbol{\nu}|^2}$ is the axial spatial frequency, q is the reconstructed axial slice index,and $\Phi(\boldsymbol{\nu}^{\pm}, \boldsymbol{\nu}_i) = \eta(\boldsymbol{\nu}^{\pm}) - \eta(\boldsymbol{\nu}_i)$ denotes the shifted axial spatial frequency term.

These terms highlight three critical features of IDT. First, the translated pupil $P(\boldsymbol{\nu} \pm \boldsymbol{\nu}_i)$ under oblique illumination enhances the reconstructed object's bandwidth up to the incoherent limit. Second, the TFs' slice-dependent exponential functions enable volumetric recovery by predicting the propagation phase from each axial slice. Finally, the real TF recovering the object's phase information exhibits asymmetric behavior aligning with observations seen in differential phase contrast [21]. In overlap regions between $\hat{I}_2$ and $\hat{I}_3$, this asymmetry removes the object's phase information and reduces the image's information content. Maintaining high resolution with minimal phase TF overlap is critical for high-throughput IDT discussed below.

With TFs for all axial slices and illuminations(Fig. 1(b)), the object volume is recovered slice-wise using Tikhonov regularization [37]. IDT's volumetric, quantitative recovery can be seen in the diatom algae reconstruction in Fig. 1(c). These reconstructions preserve high-resolution features over the full volume and highlight the high-quality 3D QPI IDT provides in a simple optical setup with linear inverse scattering models.

III. IDT High Volume Rate Methods

Conventional IDT provides high-quality 3D QPI recovery with low temporal resolution [8]. This first approach required multi-second acquisition times and hundreds of illuminations for a single measurement, which limited the technique to evaluating static objects. Here, we discuss both multiplexed IDT (mIDT) and annular IDT (aIDT) as high-throughput

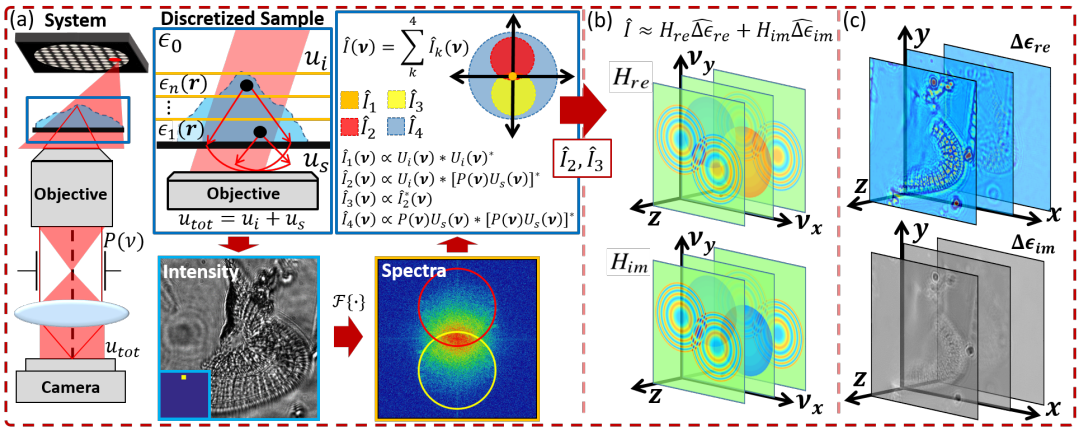

Fig. 1. (a) The IDT system schematic (Left) with the axial discretization process (Top middle), example intensity image under oblique illumination (Bottom middle), and intensity spectra breakdown (Right). (b) The IDT forward model and visualizations of the 3D real and imaginary TFs from a single oblique illumination. A 4D TF stack for all axial positions and illumination angles are required for reconstructing the object. (c) Example volumetric reconstructions of a diatom biological sample's real and imaginary permittivity contrast.

solutions enabling 3D QPI on dynamic biological samples that hold greater interest for the biological research community.

A. Multiplexed IDT

mIDT provides a software-only solution for achieving high-throughput IDT by optimally combining illuminations based on IDT's physical model. This approach is ideal for combining high-throughput IDT in multimodal computational imaging [38] and Fourier Ptychography [22] setups using generic LED arrays. The mIDT framework assumes mutually incoherent LED illumination and implements three model-based design constraints: 1) low-angle illumination removal, 2) Source position geometric constraints, and 3) poisson disk random sampling [39]. The first constraint removes low-angle illuminations (NA$\leq$0.3) that capture only low-resolution object information and lose phase features from the large overlap of $\hat{I}_2$ and $\hat{I}_3$. To prevent symmetric illumination from removing the object's phase information with overlapped TFs, the mIDT framework also restricts the available illuminations for a given image to one Fourier space quadrant (Fig. 2(a)). Finally, we randomly select LEDs within a given quadrant using poisson disk sampling [39] to maximize the recovered object bandwidth in each image. This method implements minimum geometric distances between randomly selected illuminations [39] to prevent TF overlap and enhance the recovered object bandwidth. With these constraints, we perform a randomized search procedure using a custom, non-differentiable metric that maximizes the mIDT system TF's singular value distribution (SVD) (Fig. 2(b)) [1]. Maximizing this metric maintains the bandwidth of conventional IDT using the reduced image quantity of mIDT. This dataset reduction, coupled with a camera exposure time reduction from the greater light throughput achieved with multiplexed illumination, enables high-throughput IDT.

Example reconstructions of live epithelial buccal cells are shown in Fig. 2(c) and [1]. The quantitative refractive index values of native bacteria and other particles are easily recovered in time (Fig. 2(c), Outsets) without motion artifacts. As discussed in [1], the mIDT approach is limited to 4Hz volume rates with the current setup's slow illumination hardware and exhibits object-dependent structural artifacts in the reconstruction due to the multiplexed illumination. These limitations spurred the investigation of hardware-based speed solutions discussed below.

B. Annular IDT

Annular IDT (aIDT) provides a hardware-based solution for high volume-rate IDT. The best IDT reconstruction from analyzing the IDT TFs results from using oblique illumination angles matching the objective NA, as these angles provide the greatest achievable resolution with the least phase TF overlap between $\hat{I}_2$ and $\hat{I}_3$. Such illuminations capture significant object information and can be easily achieved through the use of a ring-geometry LED array as the illumination hardware (Fig. 2(d)). In addition, this circular illumination hardware better samples the object's Fourier space [40] requiring only 8 intensity images for recovering the object's bandwidth [2]. These improvements enable high volume-rate IDT without the need for multiplexed illumination.

Example results for aIDT volumetric reconstructions are shown in Fig. 2(e). aIDT achieves hardware-limited 10Hz acquisition rates and recovers high-quality *C. elegans* worm reconstructions without motion artifacts. This reconstruction clearly recovers tissue structures including muscle walls and intestines (Fig. 2(e), brackets), lipid droplets and circular structures (white arrows), the vulva (square), and native bacteria (diamond) outside the worm. The videos in [2] further highlight the lack of motion artifacts and exhibit no structure-dependent artifacts like mIDT. This aIDT approach provides an easily implementable, high volume-rate QPI system that can be easily adopted for biological research applications.

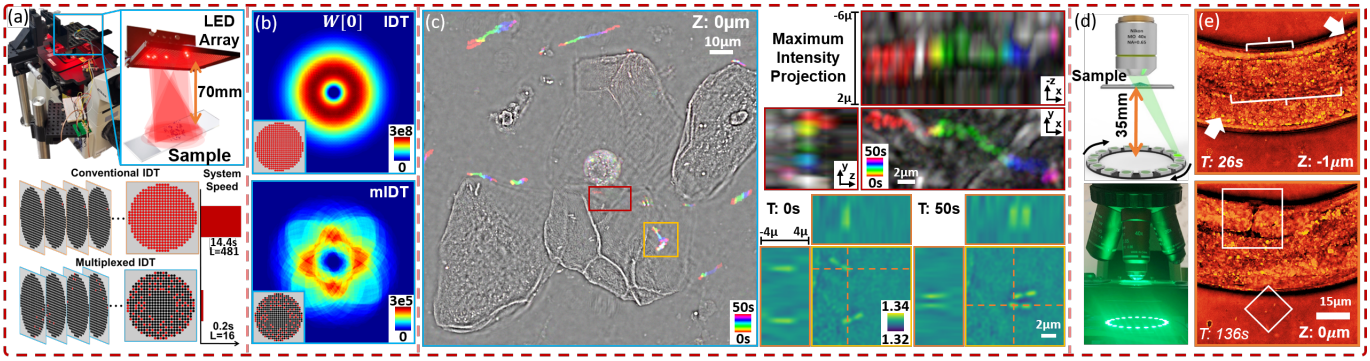

Fig. 2. (a) mIDT system with conventional and multiplexed illumination schemes, (b) example IDT and mIDT system TF SVDs, (c) mIDT time-encoded reconstruction of epithelial buccal cells. The maximum intensity projection highlights a particle's 3D movement captured with mIDT. A native bacteria's refractive index is also shown to be recovered with mIDT volumetrically at two time points. (d) The aIDT imaging setup, and (e) example *C. elegans* worm reconstructions at different depths and times capturing tissue structures including: Intestines and muscle wall (brackets), lipid droplets and high-resolution circular structures (arrows), the vulva (box), and native bacteria (diamond). Images in (a)-(c) reprinted from [1], (d)-(e) reprinted from [2].

IV. IDT Learning Techniques

Beyond high volume-rate imaging, IDT's next significant barrier is its single-scattering physical model. Such models underestimate the object's physical properties when evaluating the complex, multiple-scattering objects more commonly found in biology [2]. While multiple-scattering inverse models exist for complex object recovery and could be investigated for IDT [9], [29], their increased complexity sacrifice IDT's computationally simple implementation. Alternatively, phase recovery with deep learning methods maintain computational simplicity for complex object recovery at the cost of a "black-box" architecture with unknown reliability. To provide both computationally efficient reconstructions with reliable results, we consider a recently developed uncertainty learning framework [3] in FP as a potential approach for enhancing IDT's multiple-scattering object recovery. We discuss this method briefly below and direct the reader to [3] for greater detail.

Uncertainty learning determines the per-pixel uncertainty of a neural network by considering the network weights as probability distributions with a Bayesian neural network (BNN) [3]. The predictive distribution of phase values $\boldsymbol{y}$ the network can provide can then be evaluated based on the test input $\boldsymbol{x}^*$, model weights $\boldsymbol{w}$, and training data $(\boldsymbol{X}, \boldsymbol{Y})$ distributions

$$p(\boldsymbol{y}|\boldsymbol{x}^*, \boldsymbol{X}, \boldsymbol{Y}) = \int p(\boldsymbol{y}|\boldsymbol{x}^*, \boldsymbol{w}) p(\boldsymbol{w}|\boldsymbol{X}, \boldsymbol{Y}) d\boldsymbol{w}. \quad (3)$$

The distributions in Eq. (3) correspond to the data and model uncertainties and describe 1) the possible predictions given the learned weights and 2) the possible model weights learned from the training dataset. Quantifying these distributions evaluates the trained network's overall quality and determines whether imperfections exist in the dataset [3]. These distributions are evaluated in a per-pixel uncertainty map jointly obtained with the network's prediction (Fig. 3(a)) and correlate highly with the prediction's error with respect to the ground truth. By using this uncertainty map as a surrogate for the true prediction error, this uncertainty learning method enhances a network prediction's reliability by determining whether the prediction's features are trustworthy. For QPI, implementing uncertainty learning for recovering complex, multiple-scattering objects can provide reliable phase recovery in a computationally efficient approach without suffering from the limitations of model-based reconstruction techniques.

Predicted phase and uncertainty maps of an ethanol-fixed HeLa cell sample show this reliability analysis in Fig. 3(b). These predictions, obtained from a U-Net architecture trained to recover 2D phase maps from illumination-multiplexed intensity images, show high correlations between the uncertainty maps provided using our approach and the prediction's absolute error when compared with conventional FP reconstruction techniques. This correlation shows the uncertainty maps provide a surrogate to the absolute error when ground truth data is unavailable, and the low overall phase error indicates the network's phase prediction can provide reliable QPI measurements without the computational complexity of the FP and other iterative reconstruction methods. With future applications to IDT, this uncertainty learning approach shows significant promise for providing reliable complex object recovery.

V. Discussion and Conclusion

We presented three approaches enhancing the intensity diffraction tomography modality. Using model-based computational illumination design schemes, we showed hardware-limited 4Hz and 10Hz volume-rates drastically improving IDT's throughput for dynamic sample imaging. We discussed a recently developed uncertainty learning framework that provides reliability estimates of a neural network's prediction in QPI applications. We showed experimentally that this framework provides per-pixel uncertainty estimates of the network's prediction that can be used as a surrogate to the prediction's error compared to the ground truth. These developments in IDT and learning-based QPI show there is significant potential in providing volumetric QPI measurements of live, native complex biological samples.

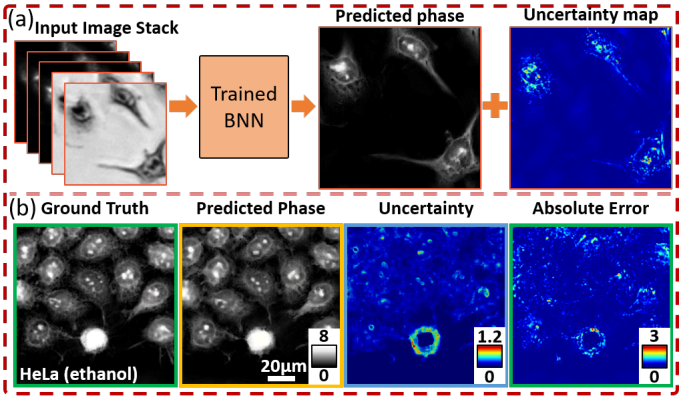

Fig. 3. (a) The phase prediction and uncertainty map pipeline using a modified U-Net for the BNN [3]. (b) Fourier Ptychography-recovered ground truth phase, BNN-predicted phase, BNN uncertainty map, and absolute error on ethanol-fixed HeLa cells. The BNN prediction's low error shows high-quality phase prediction, and the uncertainty map's correlation with the error shows its utility as a surrogate error metric. Images reprinted from [3].

REFERENCES

[1] A. Matlock and L. Tian, "High-throughput, volumetric quantitative phase imaging with multiplexed intensity diffraction tomography," *Biomed. Opt. Express*, vol. 10, no. 12, p. 6432, Nov 2019.

[2] J. Li, A. Matlock, Y. Li, Q. Chen, C. Zuo, and L. Tian, "High-speed in vitro intensity diffraction tomography," *Adv. Phot.*, vol. 1, no. 6, p. 066004, 2019.

[3] Y. Xue, S. Cheng, Y. Li, and L. Tian, "Reliable deep-learning-based phase imaging with uncertainty quantification," *Optica*, vol. 6, no. 5, p. 618, May 2019.

[4] T. Kim, R. Zhou, L. L. Goddard, and G. Popescu, "Solving inverse scattering problems in biological samples by quantitative phase imaging," *Laser & Photonics Reviews*, vol. 10, no. 1, pp. 13–39, 2016.

[5] Y. Park, C. Depeursinge, and G. Popescu, "Quantitative phase imaging in biomedicine," *Nature Photonics*, vol. 12, no. 10, p. 578, 2018.

[6] D. Jin, R. Zhou, Z. Yaqoob, and P. So, "Tomographic phase microscopy: Principles and applications in bioimaging," *J. Opt. Soc. Am. B*, vol. 34, no. 5, pp. B64–B77, 2017.

[7] L. Tian and L. Waller, "3d intensity and phase imaging from light field measurements in an led array microscope," *Optica*, vol. 2, no. 2, pp. 104–111, 2015.

[8] R. Ling, W. Tahir, H.-Y. Lin, H. Lee, and L. Tian, "High-throughput intensity diffraction tomography with a computational microscope," *Biomedical Optics Express*, vol. 9, no. 5, p. 2130, Apr 2018.

[9] W. Tahir, U. S. Kamilov, and L. Tian, "Holographic particle localization under multiple scattering," *Adv. Phot.*, vol. 1, no. 3, p. 036003, 2019.

[10] U. S. Kamilov, I. N. Papadopoulos, M. H. Shoreh, A. Goy, C. Vonesch, M. Unser, and D. Psaltis, "Learning approach to optical tomography," *Optica*, vol. 2, no. 6, pp. 517–522, 2015.

[11] V. Nandakumar, L. Kelbauskas, K. F. Hernandez, K. M. Lintecum, P. Senechal, K. J. Bussey, P. C. Davies, R. H. Johnson, and D. R. Meldrum, "Isotropic 3d nuclear morphometry of normal, fibrocystic and malignant breast epithelial cells reveals new structural alterations," *PloS one*, vol. 7, no. 1, p. e29230, 2012.

[12] Y. Park, M. Diez-Silva, G. Popescu, G. Lykotrafitis, W. Choi, M. S. Feld, and S. Suresh, "Refractive index maps and membrane dynamics of human red blood cells parasitized by plasmodium falciparum," *Proc. of the Nat. Acad. of Sciences*, vol. 105, no. 37, pp. 13 730–13 735, 2008.

[13] T. H. Nguyen, M. E. Kandel, M. Rubessa, M. B. Wheeler, and G. Popescu, "Gradient light interference microscopy for 3D imaging of unlabeled specimens," *Nature Comm.*, vol. 8, no. 1, p. 210, 2017.

[14] Z. Wang, L. Millet, M. Mir, H. Ding, S. Unarunotai, J. Rogers, M. U. Gillette, and G. Popescu, "Spatial light interference microscopy (SLIM)," *Opt. Express*, vol. 19, no. 2, pp. 1016–1026, Jan. 2011.

[15] M. Chen, L. Tian, and L. Waller, "3D differential phase contrast microscopy," *Biomed. Opt. Express*, vol. 7, no. 10, pp. 3940–3950, Oct 2016.

[16] N. Streibl, "Phase imaging by the transport equation of intensity," *Opt. Commun.*, vol. 49, no. 1, pp. 6–10, 1984.

[17] J. Li, Q. Chen, J. Sun, J. Zhang, J. Ding, and C. Zuo, "Three-dimensional tomographic microscopy technique with multi-frequency combination with partially coherent illuminations," *Biomedical Optics Express*, vol. 9, no. 6, pp. 2526–2542, 2018.

[18] J. M. Soto, J. A. Rodrigo, and T. Alieva, "Optical diffraction tomography with fully and partially coherent illumination in high numerical aperture label-free microscopy," *Applied Optics*, vol. 57, no. 1, pp. A205–A214, 2018.

[19] E. Wolf, "Three-dimensional structure determination of semi-transparent objects from holographic data," *Opt. Commun.*, vol. 1, no. 4, pp. 153–156, September/October 1969.

[20] J. M. Soto, J. A. Rodrigo, and T. Alieva, "Label-free quantitative 3d tomographic imaging for partially coherent light microscopy," *Opt. Express*, vol. 25, no. 14, pp. 15 699–15 712, 2017.

[21] L. Tian and L. Waller, "Quantitative differential phase contrast imaging in an LED array microscope," *Opt. Express*, vol. 23, no. 9, pp. 11 394–11 403, May 2015.

[22] G. Zheng, R. Horstmeyer, and C. Yang, "Wide-field, high-resolution Fourier Ptychographic microscopy," *Nat. Photonics*, vol. 7, no. 9, pp. 739–745, 2013.

[23] L. Tian, X. Li, K. Ramchandran, and L. Waller, "Multiplexed coded illumination for Fourier ptychography with an LED array microscope," *Biomed. Opt. Express*, vol. 5, no. 7, pp. 2376–2389, Jul 2014.

[24] L. Tian, Z. Liu, L.-H. Yeh, M. Chen, J. Zhong, and L. Waller, "Computational illumination for high-speed in vitro Fourier ptychographic microscopy," *Optica*, vol. 2, no. 10, pp. 904–911, 2015.

[25] S. Mehta and C. Sheppard, "Quantitative phase-gradient imaging at high resolution with asymmetric illumination-based differential phase contrast," *Opt. Lett.*, vol. 34, no. 13, pp. 1924–1926, 2009.

[26] D. Hamilton and C. Sheppard, "Differential phase contrast in scanning optical microscopy," *J. Microscopy*, vol. 133, no. 1, pp. 27–39, 1984.

[27] M. Kellman, E. Bostan, N. Repina, and L. Waller, "Physics-based learned design: Optimized coded-illumination for quantitative phase imaging," *IEEE Transactions on Computational Imaging*, 2019.

[28] R. Horstmeyer, J. Chung, X. Ou, G. Zheng, and C. Yang, "Diffraction tomography with fourier ptychography," *Optica*, vol. 3, no. 8, pp. 827–835, 2016.

[29] S. Chowdhury, M. Chen, R. Eckert, D. Ren, F. Wu, N. Repina, and L. Waller, "High-resolution 3d refractive index microscopy of multiple-scattering samples from intensity images," *Optica*, vol. 6, no. 9, pp. 1211–1219, 2019.

[30] J. Lim, A. B. Ayoub, E. E. Antoine, and D. Psaltis, "High-fidelity optical diffraction tomography of multiple scattering samples," *Light: Science & Applications*, vol. 8, no. 1, pp. 1–12, 2019.

[31] G. Barbastathis, A. Ozcan, and G. Situ, "On the use of deep learning for computational imaging," *Optica*, vol. 6, no. 8, pp. 921–943, 2019.

[32] A. Goy, G. Rughoobur, S. Li, K. Arthur, A. I. Akinwande, and G. Barbastathis, "High-resolution limited-angle phase tomography of dense layered objects using deep neural networks," *Proceedings of the National Academy of Sciences*, 2019.

[33] Y. Rivenson, Y. Zhang, H. Günaydın, D. Teng, and A. Ozcan, "Phase recovery and holographic image reconstruction using deep learning in neural networks," *Light: Science & Applications*, vol. 7, no. 2, p. 17141, 2018.

[34] T. Nguyen, Y. Xue, Y. Li, L. Tian, and G. Nehmetallah, "Deep learning approach for Fourier ptychography microscopy," *Opt. Express*, vol. 26, no. 20, p. 26470, Sep 2018.

[35] Z. Wu, Y. Sun, A. Matlock, J. Liu, L. Tian, and U. S. Kamilov, "Simba: Scalable inversion in optical tomography using deep denoising priors," *arXiv preprint arXiv:1911.13241*, 2019.

[36] M. Born and E. Wolf, *Principles of Optics*, 7th ed. Cambridge Univ. Press, 1999.

[37] M. Bertero and P. Boccacci, *Introduction to inverse problems in imaging*. Taylor & Francis, 1998.

[38] Z. Liu, L. Tian, S. Liu, and L. Waller, "Real-time brightfield, darkfield, and phase contrast imaging in a light-emitting diode array microscope," *J. of Biomed. Opt.*, vol. 19, no. 10, pp. 106 002–106 002, 2014.

[39] R. Bridson, "Fast poisson disk sampling in arbitrary dimensions." in *SIGGRAPH sketches*, 2007, p. 22.

[40] K. Guo, S. Dong, P. Nanda, and G. Zheng, "Optimization of sampling pattern and the design of fourier ptychographic illuminator," *Opt. express*, vol. 23, no. 5, pp. 6171–6180, 2015.